Increased Excited State Metallicity in Neutral Cr_2O_n Clusters (n < 5) Upon Sequential Oxidation

Jacob M. Garcia[1,2] and Scott G. Sayres[1,2,*]

[1]School of Molecular Sciences, Arizona State University, Tempe, AZ 85287

[2]Biodesign Center for Applied Structural Discovery, Arizona State University, Tempe, AZ 85287

Excited state lifetimes of neutral Cr_2O_n (n < 5) clusters were measured using femtosecond pump-probe spectroscopy. Density functional theory calculations reveal that the excited state dynamics are correlated with changes in the cluster's electronic structure with increasing oxidation. Upon absorption of a UV (400 nm) photon, the clusters exhibit features attributed to three separate relaxation processes. All clusters exhibit similar sub-picosecond lifetimes, attributed to vibrational relaxation. However, the ~30 fs transient signal fraction grows linearly with oxidation, matching the amount of O to Cr charge transfer character of the photoexcitation and highlighting a gradual transition between semiconducting and metallic behavior at the molecular level. A long-lived (>2.5 ps) response is recorded only in clusters with significant d-electron character, suggesting that adiabatic relaxation back to the ground state is efficient in heavily oxidized clusters, due to the presence of terminal O atoms. The simple picture of sequential oxidation of Cr_2O_n reveals a linear variation in the contributions of each relaxation component to the total transient signals, therefore opening possibilities for the design of new molecular spintronic materials.

Chromium oxides are widely studied for their magnetic and electronic properties, commonly being employed in magnetic storage devices. In particular, CrO_2 is a well-established half-metal with the highest spin polarization of any material,[1–3] attracting substantial research interest for potential spintronics and data storage applications. This unique half-metallic property in CrO_2 arises from a large energy spin gap, where the delocalized majority spin states close to the Fermi energy are metallic and the minority spins are semiconducting or insulating.[4] Therefore, isolating and controlling the separate spin states to induce (anti)ferromagnetic properties are of increasing interest. The ultimate speed at which its magnetic states can be manipulated is of key importance due to its attractive potential for use in spintronic heterostructures and magnetoelectronic devices requiring spin polarization, such as magnetic tunnel junctions[5] and spin valves.[6] The photodriven process of (de)magnetization and optical spin transport can be manipulated with light on the femtosecond timescale, but follows a complex route of intermediate states accompanying changes in spin and lattice parameters, and is not fully understood.[7] Despite its relevance to industrial technology, controlling the magnetic states in chromium oxides requires more detailed information on oxygen-dependent electronic state dynamics and electron transport.

Atomically precise clusters provide a superior avenue to examine the factors affecting the electronic properties of chromium oxide. Additionally, chromium oxide clusters may be uniquely suitable for spintronics due to a large array of energetically competitive spin configurations.[8–11] In particular, Cr_2O_n clusters have been heavily studied both experimentally and theoretically,[9–13] showing large changes in electronic structure with oxygen content via photoelectron spectroscopy (PES),[9,12,13] and structures in agreement with vibrationally resolved IR spectroscopy.[14–16] The electronic structures of Cr_2O_n clusters arise from a unique mixing of Cr half-filled s- and d-orbitals ($3d^54s^1$) with O 2p-orbitals. The properties of chromium oxides are driven partially by superexchange coupling,[8,17] suggesting the charge-transport processes are adiabatic in nature. Manipulation of spin in antiferromagnetic (AF) Cr_2O_3 bulk materials follows several relaxation channels dependent on excitation energy, proceeding over hundreds of femtoseconds to picoseconds.[7,18,19] However, the mixing of Cr and O electrons and their effect on the lifetimes of accessible magnetic states are still not well understood and may improve the manipulation of chromium oxide materials.

Here, we report the excited state transient signals of neutral Cr_2O_n (n = 0-4) clusters using two-color pump-probe spectroscopy and apply theoretical calculations to understand the increasing metallic behavior as a function of sequential oxidation. A time-of-flight mass spectrometer (TOF-MS)[20,21] coupled to synchronized sub-35 fs laser pulses was employed to measure the excited state lifetimes of neutral Cr oxide clusters. A single 400 nm (3.1 eV) pump photon initiates a charge transfer and relaxation mechanism that is probed through ionization by a synchronized strong-field 800 nm (1.55 eV) probe beam. This simplified study of sequential oxidation of Cr_2 reveals new insights to the role of electron-electron (e-e) scattering and formation of metallic behavior in chromium oxides, similar to the half-metal quality of CrO_2.

The transient signals of Cr_2O_n (n < 5) reveal three distinct relaxation mechanisms that change with additional O atoms (Figure 1). An instantaneous decay (on the timescale of the laser pulse, τ_1 = 30 fs) is attributed to e-e scattering correlated to the ligand-to-metal charge transfer (LMCT), or excitation from O-2p to Cr-3d orbitals. A sub-ps (τ_2) relaxation is attributed to vibrational relaxation of the initially formed charge-transfer state (electron-vibration relaxation). Finally, a plateau function

represents a long-lived state (>2.5 ps) that is accessed only in sub-oxide clusters.
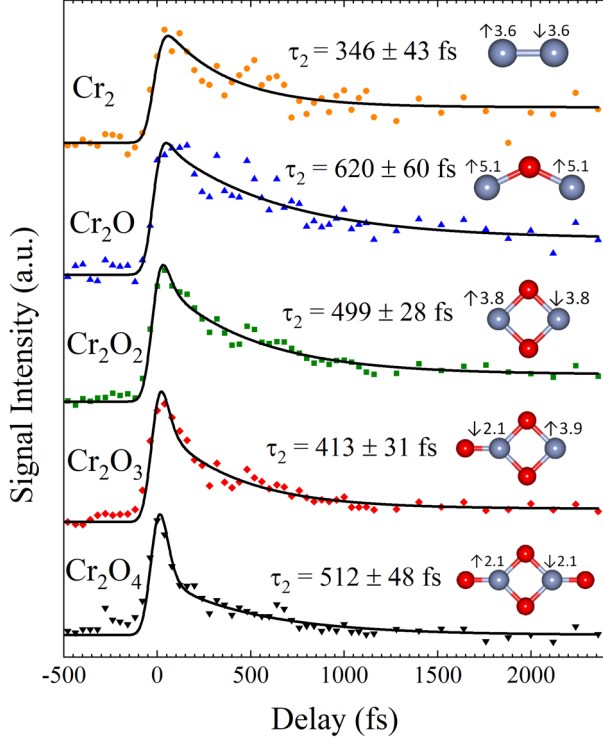

Figure 1: Transient signals of the change in ionized neutral Cr_2O_n (n = 0-4) clusters with probe delay, shown with total fits, ground state geometry, local magnetic moments and sub-picosecond lifetime (τ_2).

The Cr_2O_n clusters all exhibit similar instantaneous (τ_1) and sub-ps (τ_2) lifetimes. However, a change in amplitudes of the three fitting functions in each total transient signal with O content is revealed. The fraction of each fitting function amplitude of the total signal is represented as κ_1 (τ_1), κ_2 (τ_2), and δ (plateau function). The lifetimes and fitting coefficients for each cluster are shown in Table 1. The relative contributions of the various mechanisms change almost linearly with O content (Figure 2). The κ_1 component is not present for Cr_2 but grows to account for 84% of the signal in Cr_2O_4. In contrast, the κ_2 and δ values compose ~70% and ~30% of the total signal for Cr_2, respectively, and both decrease nearly linearly with oxidation.

In metals, excess optically applied energy dissipates through e-e scattering within 10s of fs due to strong interactions between delocalized electrons. Limited excited state lifetime measurements have been reported for pure metal clusters, and range from ~20-200 fs,[22–24] comparable to the bulk values. In contrast, long lifetimes of electron-hole excitations are characteristic of semiconductors. Metal oxide clusters contain a larger splitting of the molecular orbitals (lower density of states), which decreases the number of unoccupied levels within the excitation energy, greatly reducing relaxation rates (longer lifetime). For example, the excited state lifetimes for $(TiO_2)_n$,[21] $(ZnO)_n$[25] and $(FeO)_n$[20] clusters depend strongly on both cluster size and charge carrier localization. The instantaneous O-2p to Cr-3d e-e scattering processes (κ_1 contribution) recorded in Cr_2O_n clusters increases with oxidation (Figure 2) and suggests that they become more metallic with increasing oxidation. This is a counterintuitive result until considering that the clusters are approaching the stoichiometry of the bulk half-metal, CrO_2.
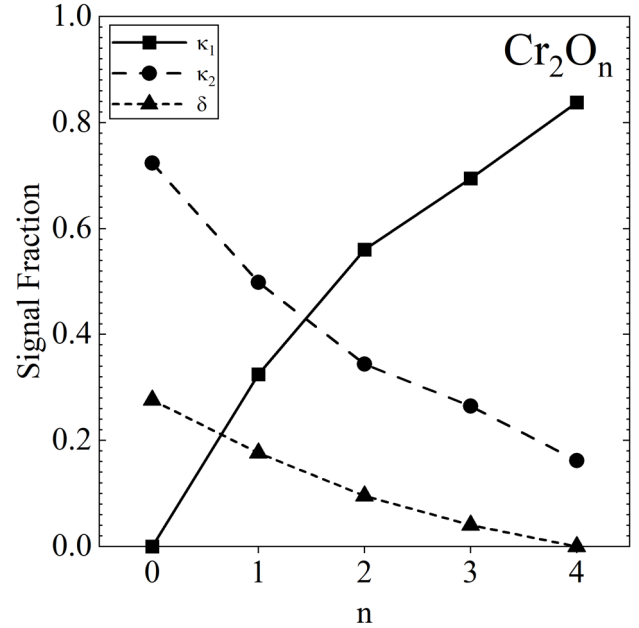

Figure 2: Plot of κ_1 (solid, squares), κ_2 (long dash, circles) and δ (short dash, triangles) of the neutral Cr_2O_n (n = 0-4) clusters.

Table 1: Lifetimes (τ_2), signal fractions of τ_1 (κ_1), τ_2 (κ_2) and long-lived plateau (δ) functions, and percent ligand-to-metal charge transfer (LMCT) for Cr_2O_n (n < 5) clusters.

Cluster	τ_2 (fs)	κ_1	κ_2	δ	LMCT
Cr_2	346 ± 43	0	0.724	0.276	0%
Cr_2O	620 ± 60	0.325	0.498	0.177	17%
Cr_2O_2	499 ± 28	0.560	0.344	0.095	31%
Cr_2O_3	413 ± 31	0.695	0.265	0.040	54%
Cr_2O_4	512 ± 48	0.838	0.162	0	63%

Insights on the relaxation dynamics are provided by changes in the theoretical electronic structure of clusters with oxidation. Due to the accuracy previously demonstrated in Cr oxide clusters,[11,26] we employ density functional theory (DFT) calculations to calculate the geometries, and time-dependent DFT to determine excited states of chromium oxide clusters (Supplemental Information). In Cr_2O_n clusters, the first two O atoms bridge between the Cr atoms, and subsequent O atoms attach to the Cr atoms while maintaining a planar geometry, in agreement with previous calculations (Figure 1).[10,11,27] Electronic superexchange between Cr and O atoms in Cr_2O_n clusters (n = 1-4) makes them antiferromagnetically (AF) coupled, except for Cr_2O which is ferromagnetically (FM) coupled. Although the FM state of Cr_2O_3 has been suggested to be degenerate,[9,10,16,27] the AF state is 0.5 eV lower in our calculations. Valence orbitals are Cr-3d dominated, with O-2p orbitals becoming important for high energy excitations or in clusters containing many O atoms. With increasing oxidation, the local magnetic moment on the Cr atoms steadily decreases from 5.1 μB in Cr_2O to 2.1 μB

in Cr_2O_4, nearly matching the magnetic moment per Cr atom in bulk (~2.0 μB).[4,28]

Photoexcitation with a 3.1 eV pump photon shifts from d-d transitions between Cr atoms toward more LMCT character in Cr_2O_n clusters (Figure S1). As O atoms are included in the cluster, the Cr 3d-based spectral features diminish and the excited state shifts towards increasing involvement of O-2p orbitals with oxidation[12] as a result of charge transfer from Cr to O. The photoexcitation of Cr_2 is primarily a d-d transition in agreement with the transient signal that contains no κ_1 component and leads to an elongated bond. The excited state of Cr_2O contains up to 17% LMCT density and the transient signal contains 33% κ_1. The increased LMCT character (31%) of the photoexcited state in Cr_2O_2 matches the increased κ_1 (56%) of the total transient signal. Several excited states overlap around ~3.1 eV for Cr_2O_3, involving a maximum 54% LMCT character and increased experimental transient signal of 70% κ_1. Photoexcitation in Cr_2O_4 is up to 63% LMCT matching the largest κ_1 (84%) of the measured clusters and also contains no δ contribution. The LMCT projects an electron back onto the Cr-3d orbitals, inducing a rapid scattering on the few-fs timescale, similar to metallic excitations. In all cases, the bridging O act as electron donors, but the terminal O atoms act as both donors and acceptors. The electronic structures show a near-linear increase in the percent LMCT between O-2p and Cr-3d orbitals with oxidation (Figure 3), in excellent agreement to the increase in the measured κ_1 contribution.
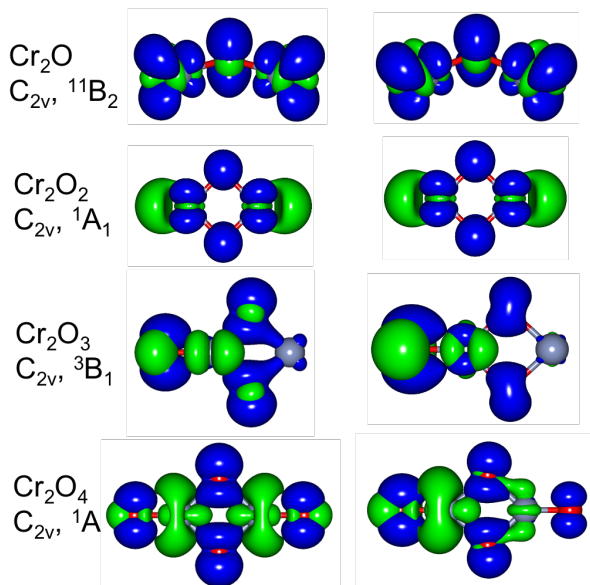

Figure 3: Vertical (left) and adiabatically relaxed (right) excited state transition densities for Cr_2O_n, (n = 1-4) clusters, presented at an isodensity of $0.002/Å^3$. Electron and hole density is shown in green and blue, respectively. Cr atoms are gray, and O are red.

Following vertical excitation, the clusters relax adiabatically, aligning with changes in their experimental transients. A linear decrease in δ with oxidation reveals that additional degrees of vibrational freedom improve each cluster's propensity to return to the ground state as vibrationally hot species. Although τ_2 is similar for all clusters, Cr_2O is ~20% longer (620 ± 60 fs), which may be related to FM coupling and an activated bending mode. In particular, terminal O atoms are well known to facilitate relaxation to the ground state through conical intersections,[29] and therefore reduces δ. The nuclear rearrangement for both Cr_2O_3 and Cr_2O_4 is primarily localized to the bending and stretching motions of the terminal O atoms. Photoexcitation of Cr_2O_3 prepares a localized electron on the tri-coordinated Cr atom, while the other Cr is not involved due to the asymmetric O distribution in the cluster. Photoexcitation of Cr_2O_4 extends the bond length of one terminal O. Thus, Cr_2O_3 contains only 4% δ, while δ is absent from the transient signal of Cr_2O_4, revealing efficient recombination.

Our results suggest that a fully oxidized Cr_2O_6 cluster that is void of d electrons will convert all photoexcited energy into vibrational energy within 10s of fs, similar to metallic systems. This inversed (counterintuitive) metallic behavior is explained by the transition from delocalized electronic states to strongly ionic LMCT upon oxidation, similar to the half-metal behavior of bulk CrO_2. Long-lived states are only present in chromium oxides that contain O vacancies, suggesting a single-crystalline bulk material may rapidly convert photonic excitation into heat within 10s of fs. The ultrafast dynamics reported herein show half-metal behavior at the molecular level. Such clusters can be formed over a range of compositions and stoichiometries, enabling a wide variation in magnetic behaviors and novel molecular spintronics materials.

In conclusion, we report time-resolved excitation experiments of neutral Cr_2O_n clusters and show that the relative contribution of three separate pathways changes almost linearly with oxidation. The involvement of the near instantaneous, or metallic relaxation component, is related to the theoretically determined electronic properties. The lifetimes show that LMCT excitations relax on an almost-instantaneous timescale and that d-d excitations relax on a sub-ps timescale. Significant long-lived excited states are only observed in suboxide systems, suggesting that carrier recombination is efficient only in closed systems. This simple picture of sequential oxidation reveals a trend in the excited state dynamics related to a shifting metallic behavior with O character. Studies on larger systems may help develop rules to control magnetic interactions, with similar trends observed in our experimental signals of Cr_3O_n and Cr_4O_n clusters that will be detailed in a subsequent manuscript. Insights from these atomically precise chromium oxide systems can be applied to the design of novel photoactive materials.

SUPPORTING INFORMATION

Computational methods and properties including optimized ground state cluster geometries. Table S1 shows the elemental contributions to the excited state and related LMCT character. The SI material is free of charge via the Internet at http://pubs.acs.org.

Corresponding Author

*Scott.Sayres@asu.edu

Author Contributions

S.G.S. and J.M.G. designed the experiments. J.M.G. performed the ultrafast pump-probe spectroscopy, and J.M.G. and S.G.S. wrote the paper.

References

(1)   Müller, G. M.; Walowski, J.; Djordjevic, M.; Miao, G. X.; Gupta, A.; Ramos, A. V; Gehrke, K.; Moshnyaga, V.; Samwer, K.; Schmalhorst, J.; et al. Spin Polarization in Half-Metals

Probed by Femtosecond Spin Excitation. *Nat. Mater.* **2009**, *8*, 56–61.

(2) Heffernan, K. H.; Yu, S.; Deckoff-Jones, S.; Zhang, X.; Gupta, A.; Talbayev, D. Role of Spin Fluctuations in the Conductivity of CrO$_2$. *Phys. Rev. B* **2016**, *93*, 165143.

(3) Solovyev, I. V; Kashin, I. V; Mazurenko, V. V. Mechanisms and Origins of Half-Metallic Ferromagnetism in CrO$_2$. *Phys. Rev. B - Condens. Matter Mater. Phys.* **2015**, *92*, 144407.

(4) Coey, J. M. D.; Venkatesan, M. Half-Metallic Ferromagnetism: Example of CrO$_2$ (Invited). *J. Appl. Phys.* **2002**, *91*, 8345–8350.

(5) Leo, T.; Kaiser, C.; Yang, H.; Parkin, S. S. P.; Sperlich, M.; Güntherodt, G.; Smith, D. J. Sign of Tunneling Magnetoresistance in CrO$_2$-Based Magnetic Tunnel Junctions. *Appl. Phys. Lett.* **2007**, *91*.

(6) Singh, A.; Voltan, S.; Lahabi, K.; Aarts, J. Colossal Proximity Effect in a Superconducting Triplet Spin Valve Based on the Half-Metallic Ferromagnet CrO$_2$. *Phys. Rev. X* **2015**, *5*, 1–6.

(7) Guo, F.; Zhang, N.; Jin, W.; Chang, J. Model of Ultrafast Demagnetization Driven by Spin-Orbit Coupling in a Photoexcited Antiferromagnetic Insulator Cr$_2$O$_3$. *J. Chem. Phys.* **2017**, *146*, 244502.

(8) Paul, S.; Misra, A. Magnetic Properties of Cr$_2$O$_n^-$ Clusters: A Theoretical Study. *J. Mol. Struct. THEOCHEM* **2009**, *895*, 156–160.

(9) Tono, K.; Terasaki, A.; Ohta, T.; Kondow, T. Chemically Induced Ferromagnetic Spin Coupling: Electronic and Geometric Structures of Chromium-Oxide Cluster Anions, Cr$_2$O$_n^-$ (n= 1-3), Studied by Photoelectron Spectroscopy. *J. Chem. Phys.* **2003**, *119*, 11221–11227.

(10) Reddy, B.; Khanna, S.; Ashman, C. Oscillatory Magnetic Coupling in Cr$_2$O$_n$ (n=1-6) Clusters. *Phys. Rev. B - Condens. Matter Mater. Phys.* **2000**, *61*, 5797–5801.

(11) Gutsev, G. L.; Bozhenko, K. V; Gutsev, L. G.; Utenyshev, A. N.; Aldoshin, S. M. Transitions from Stable to Metastable States in the Cr$_2$O$_n$ and Cr$_2$O$_n^-$ Series, n = 1-14. *J. Phys. Chem. A* **2017**, *121*, 845–854.

(12) Zhai, H. J.; Wang, L. S. Probing the Electronic Properties of Dichromium Oxide Clusters Cr$_2$O$_n^-$ (n=1-7) Using Photoelectron Spectroscopy. *J. Chem. Phys.* **2006**, *125*, 164315.

(13) Tono, K.; Terasaki, A.; Ohta, T.; Kondow, T. Chemical Control of Magnetism: Oxidation-Induced Ferromagnetic Spin Coupling in the Chromium Dimer Evidenced by Photoelectron Spectroscopy. *Phys. Rev. Lett.* **2003**, *90*, 4.

(14) Zhang, Q. Q.; Zhao, Y.; Gong, Y.; Zhou, M. Matrix Isolation Infrared Spectroscopic and Theoretical Study of Dinuclear Chromium Oxide Clusters: Cr$_2$O$_n$ (n = 2, 4, 6) in Solid Argon. *J. Phys. Chem. A* **2007**, *111*, 9775–9780.

(15) Bondybey, V. E.; English, J. H. Electronic Structure and Vibrational Frequency of Cr$_2$. *Chem. Phys. Lett.* **1983**, *94*, 443–447.

(16) Veliah, S.; Xiang, K. H.; Pandey, R.; Recio, J. M.; Newsam, J. M. Density Functional Study of Chromium Oxide Clusters: Structures, Bonding, Vibrations, and Stability. *J. Phys. Chem. B* **1998**, *102*, 1126–1135.

(17) Pham, L. N.; Claes, P.; Lievens, P.; Jiang, L.; Wende, T.; Asmis, K. R.; Nguyen, M. T.; Janssens, E. Geometric Structures and Magnetic Interactions in Small Chromium Oxide Clusters. *J. Phys. Chem. C* **2018**, *122*, 27640–27647.

(18) Sala, V. G.; Dal Conte, S.; Miller, T. A.; Viola, D.; Luppi, E.; Véniard, V.; Cerullo, G.; Wall, S. Resonant Optical Control of the Structural Distortions That Drive Ultrafast Demagnetization in Cr$_2$O$_3$. *Phys. Rev. B* **2016**, *94*.

(19) Satoh, T.; Van Aken, B. B.; Duong, N. P.; Lottermoser, T.; Fiebig, M. Ultrafast Spin and Lattice Dynamics in Antiferromagnetic Cr$_2$O$_3$. *Phys. Rev. B - Condens. Matter Mater. Phys.* **2007**, *75*.

(20) Garcia, J. M.; Shaffer, R. E.; Sayres, S. G. Ultrafast Pump-Probe Spectroscopy of Neutral Fe$_n$O$_m$ Clusters (n, m < 16). *Phys. Chem. Chem. Phys.* **2020**, *22*, 24624–24632.

(21) Garcia, J. M.; Heald, L. F.; Shaffer, R. E.; Sayres, S. G. Oscillation in Excited State Lifetimes with Size of Sub-Nanometer Neutral (TiO$_2$)$_n$ Clusters Observed with Ultrafast Pump–Probe Spectroscopy. *J. Phys. Chem. Lett.* **2021**, *12*, 4098–4103.

(22) Pontius, N.; Bechthold, P. S.; Neeb, M.; Eberhardt, W. Time-Resolved Photoelectron Spectra of Optically Excited States in Pd$_3^-$. *J. Electron Spectros. Relat. Phenomena* **2001**, *114–116*, 163–167.

(23) Pontius, N.; Lüttgens, G.; Bechthold, P. S.; Neeb, M.; Eberhardt, W. Size-Dependent Hot-Electron Dynamics in Small Pd$_n^-$ Clusters. *J. Chem. Phys.* **2001**, *115*, 10479–10483.

(24) Pontius, N.; Bechthold, P. S.; Neeb, M.; Eberhardt, W. Ultrafast Hot-Electron Dynamics Observed in Pt$_3^-$ Using Time-Resolved Photoelectron Spectroscopy. *Phys. Rev. Lett.* **2000**, *84*, 1132–1135.

(25) Heinzelmann, J.; Koop, A.; Proch, S.; Ganteför, G. F.; Łazarski, R.; Sierka, M. Cage-Like Nanoclusters of ZnO Probed by Time-Resolved Photoelectron Spectroscopy and Theory. *J. Phys. Chem. Lett.* **2014**, *5*, 2642–2648.

(26) Gutsev, G. L.; Jena, P.; Zhai, H. J.; Wang, L. S. Electronic Structure of Chromium Oxides, CrO$_n^-$ and CrO$_n$ (n=1-5) from Photoelectron Spectroscopy and Density Functional Theory Calculations. *J. Chem. Phys.* **2001**, *115*, 7935–7944.

(27) Wang, Y.; Gong, X.; Wang, J. Comparative DFT Study of Structure and Magnetism of TM$_n$O$_m$ (TM = Sc-Mn, n = 1-2, m = 1-6) Clusters. *Phys. Chem. Chem. Phys.* **2010**, *12*, 2471–2477.

(28) Huang, D. J.; Jeng, H. T.; Chang, C. F.; Guo, G. Y.; Chen, J.; Wu, W. P.; Chung, S. C.; Shyu, S. G.; Wu, C. C.; Lin, H. J.; et al. Orbital Magnetic Moments of Oxygen and Chromium in CrO$_2$. *Phys. Rev. B - Condens. Matter Mater. Phys.* **2002**, *66*, 1–5.

(29) Peng, W. T.; Fales, B. S.; Shu, Y.; Levine, B. G. Dynamics of Recombination: Via Conical Intersection in a Semiconductor Nanocrystal. *Chem. Sci.* **2018**, *9*, 681–687.

4

Insert Table of Contents artwork here
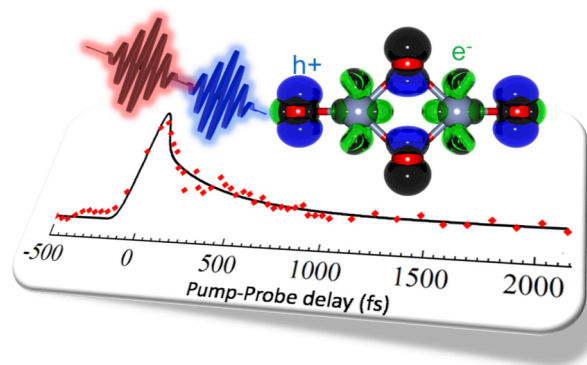
Increased Excited State Metallicity in Neutral Cr$_2$O$_n$ Clusters (n < 5) Upon Sequential Oxidation

Jacob M. Garcia[1,2] and Scott G. Sayres[1,2,*]

[1]School of Molecular Sciences, Arizona State University, Tempe, AZ 85287
[2]Biodesign Center for Applied Structural Discovery, Arizona State University, Tempe, AZ 85287

A time-of-flight mass spectrometer (TOF-MS)[1,2] coupled to synchronized femtosecond laser pulses was employed to measure the excited state lifetimes of neutral Cr oxide clusters. Laser intensities (pump = 4.8×10^{14} W/cm^2 and probe = 3.3×10^{15} W/cm^2) were minimized to eliminate ion signal from individual pulses. Cr_2O_n clusters have high O dissociation energies,[3] and therefore are stable with absorption of a 3.1 eV pump photon. The excited states are then probed through strong-field ionization with the 800 nm beam, and the measured ion signal intensity is proportional to the neutral population remaining in the excited state.

The ground state geometries of Cr_2O_n clusters were optimized at the density functional theory (DFT) level within the Gaussian16[4] software suite using the GGA functional uBPW91 with the standard 6-311G+ (3d) basis set. This configuration has previously shown to be highly accurate for the structures and energies of chromium oxide clusters.[3,5] The minimum state geometries were used as input for single point TD-DFT calculations to account for the excited state characteristics. However, excited state energies, oscillator strengths and charge-transfer characters are strongly dependent on the choice of exchange-correlation (XC) potential. A well-known charge transfer (CT) problem exists in TD-DFT, where XC potentials with no or low percentages of Hartree−Fock like exchange fail to correctly account for the excitation energies of CT states.[6] The Coulomb attenuating method (CAM)-B3LYP contains 19% and 65% Hartree-Fock exchange in the short range and the long range, respectively, and therefore balances the local excitation and charge transfer. The CAM-B3LYP XC has been shown to give accurate results for the excited state energies of TiO_2,[7,8] and pure metallic[9] clusters.

The first 200 excited states of each cluster in the Cr_2O_n (n< 5) series were then calculated using the Time-Dependent density functional theory (TD-DFT) using both uBPW91 and CAM-B3LYP

with the standard 6-311G+ (3d) basis set and using the ground state geometries determined from uBPW91 as input. An excited state population analysis was performed to determine the elemental contributions to the excited state. The excited state CT character for both basis sets are shown in Figure S1.

In general, the CAM-B3LYP and BPW91 excited state are qualitatively similar. The onset of strong O-2p to Cr-3d transitions shifts to lower energies with the inclusion of O atoms. For example, according to BPW91, the LMCT states for Cr_2O begins around 5 eV, and gradually shifts to around 3 eV for Cr_2O_4. Cr_2 is not shown as there cannot be a change in electron density over the Cr atoms. Cam-B3LYP shows less of a Cr to O transition (less negative values), and instead demonstrates a more realistic charge transfer primarily from O to Cr atoms. Results from both basis sets show that the maximum percent LMCT character near the pump laser energy increases linearly with O atoms, in agreement with the trend in experimental fitting coefficients.

The energies of the LMCT states are overestimated in both basis sets, but are more energetically accessible in CAM-B3LYP. Further, the broad bandwidth of the ~30 fs laser pulse accesses excited states near 3.1 eV. Thus, we selected the excited state molecular orbitals with the largest LMCT value within the green box presented in Figure S1 for analysis.
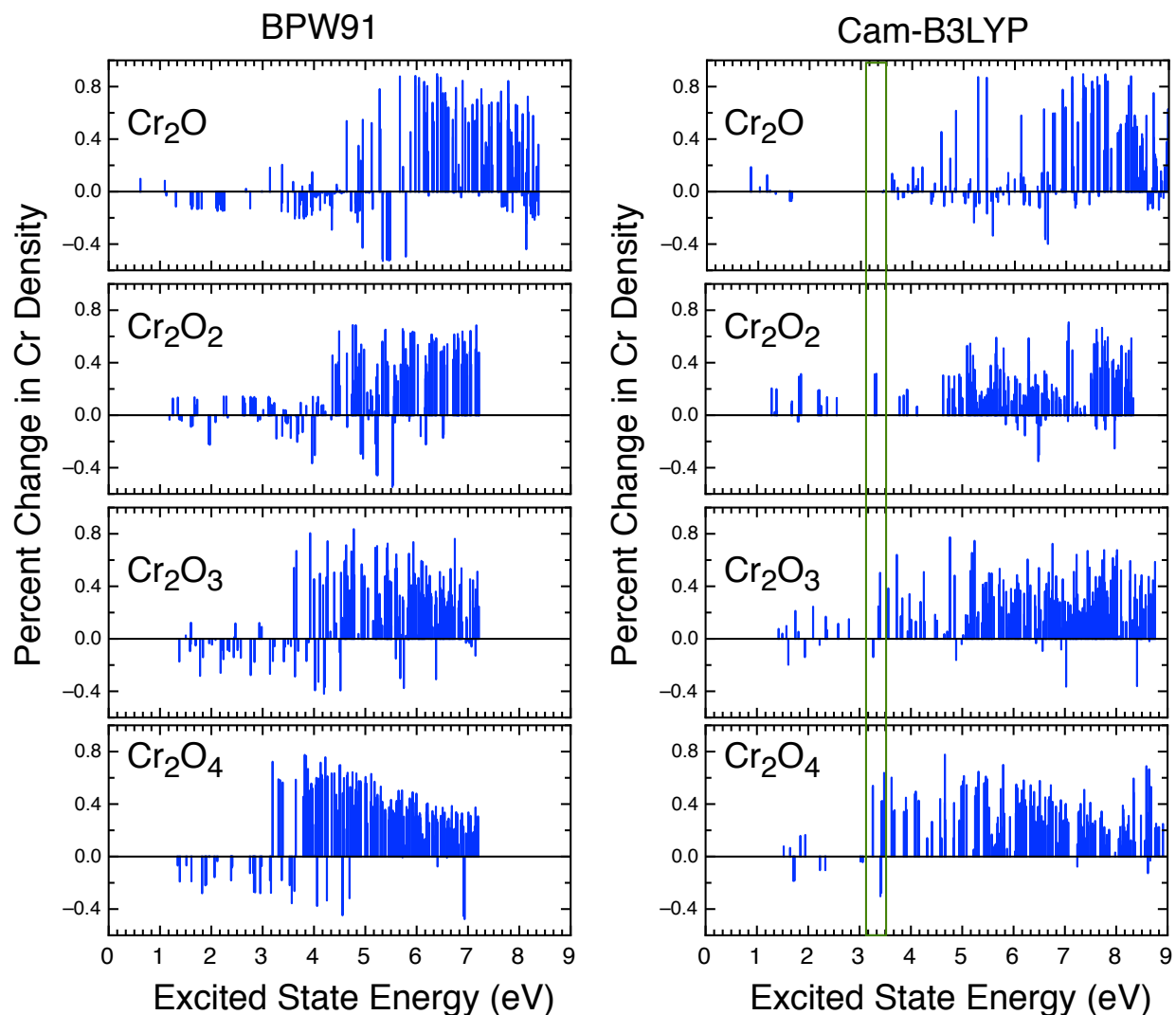
Figure S1: Percent change in electron density of the Cr atoms with photoexcitation for BPW91 (left) and CAM-B3LYP (right). Note, a positive number indicates that electron density is moving from O to Cr, whereas a negative number indicates electron density is moving from Cr to O. A small value indicates a large contribution of electron density shifting between Cr atoms. The green box represents range of excited states accessible by the pump beam.

The cartesian coordinates for the optimized ground states for the Cr_2O_n (n<5) clusters at the

DFT-uBPW91 and 6311G+(d) basis set are presented below.

$\underline{Cr_2}$
Cr   0.560590   0.695509   2.352643
Cr   0.124346   0.238736   0.716959

Cr₂O

Cr	1.624713	-0.111270	-0.000000
Cr	-1.624713	-0.111866	0.000000
O	0.000000	0.669406	-0.000000

Cr₂O₂

Cr	0.000028	0.000002	1.256118
O	-0.000001	1.326313	0.002498
O	-0.000001	-1.326313	0.002503
Cr	-0.000026	-0.000002	-1.251117

Cr₂O₃

Cr	0.000037	-1.598831	0.000000
Cr	0.000000	0.958341	0.000000
O	1.284044	-0.311354	0.000000
O	-1.283608	-0.309936	0.000000
O	-0.000546	2.542758	0.000000

Cr₂O₄

Cr	1.296014	-0.000187	-0.001464
O	-0.000238	1.254267	-0.006441
O	-0.000056	-1.254066	-0.006311
O	-2.874588	-0.000600	0.016680
O	2.874685	0.000114	0.013332
Cr	-1.295948	0.000282	-0.004290

(1)   Garcia, J. M.; Shaffer, R. E.; Sayres, S. G. Ultrafast Pump-Probe Spectroscopy of Neutral Fe$_n$O$_m$ Clusters (n, m < 16). *Phys. Chem. Chem. Phys.* **2020**, *22*, 24624–24632.

(2)   Garcia, J. M.; Heald, L. F.; Shaffer, R. E.; Sayres, S. G. Oscillation in Excited State Lifetimes with Size of Sub-Nanometer Neutral (TiO$_2$)$_n$ Clusters Observed with Ultrafast Pump–Probe Spectroscopy. *J. Phys. Chem. Lett.* **2021**, *12*, 4098–4103.

(3)   Gutsev, G. L.; Bozhenko, K. V; Gutsev, L. G.; Utenyshev, A. N.; Aldoshin, S. M. Transitions from Stable to Metastable States in the Cr$_2$O$_n$ and Cr$_2$O$_n^-$ Series, n = 1-14. *J. Phys. Chem. A* **2017**, *121*, 845–854.

(4)   Frisch, M. J.; Trucks, G. W.; Schlegel, H. B.; Scuseria, G. E.; Robb, M. A.; Cheeseman, J. R.; Scalmani, G.; Barone, V.; Mennucci, B.; Petersson, G. A.; et al. Gaussian16 (Revision C.01), Gaussian Inc. Wallingford CT. 2016.

(5)   Gutsev, G. L.; Jena, P.; Zhai, H. J.; Wang, L. S. Electronic Structure of Chromium Oxides, CrO$_n^-$ and CrO$_n$ (n=1-5) from Photoelectron Spectroscopy and Density Functional Theory Calculations. *J. Chem. Phys.* **2001**, *115*, 7935–7944.

(6)   Peach, M. J. G.; Benfield, P.; Helgaker, T.; Tozer, D. J. Excitation Energies in Density Functional Theory: An Evaluation and a Diagnostic Test. *J. Chem. Phys.* **2008**, *128*, 044118.

(7)   Berardo, E.; Hu, H. S.; Van Dam, H. J. J.; Shevlin, S. A.; Woodley, S. M.; Kowalski, K.; Zwijnenburg, M. A. Describing Excited State Relaxation and Localization in TiO_2 Nanoparticles Using TD-DFT. *J. Chem. Theory Comput.* **2014**, *10*, 5538–5548.

(8)   Berardo, E.; Hu, H. S.; Shevlin, S. A.; Woodley, S. M.; Kowalski, K.; Zwijnenburg, M. A. Modeling Excited States in TiO_2 Nanoparticles: On the Accuracy of a TD-DFT Based Description. *J. Chem. Theory Comput.* **2014**, *10*, 1189–1199.

(9)   Rabilloud, F. UV-Visible Absorption Spectra of Metallic Clusters from TDDFT Calculations. *Eur. Phys. J. D* **2013**, *67*.